A&A 553, A3 (2013)
DOI: 10.1051/0004-6361/201321207

Astronomy & Astrophysics

Spatially resolved, high-spectral resolution observation of the K giant Aldebaran in the CO first overtone lines with VLTI/AMBER⋆

K. Ohnaka

Max−Planck−Institut für Radioastronomie, Auf dem Hügel 69, 53121 Bonn, Germany
e-mail: kohnaka@mpifr.de

Received 31 January 2013 / Accepted 9 March 2013

ABSTRACT

Aims. We present a high-spatial and high-spectral resolution observation of the well-studied K giant Aldebaran with AMBER at the Very Large Telescope Interferometer (VLTI). Our aim is to spatially resolve the outer atmosphere (so-called MOLsphere) in individual CO first overtone lines and derive its physical properties, which are important for understanding the mass-loss mechanism in normal (i.e., non-Mira) K−M giants.

Methods. Aldebaran was observed between 2.28 and 2.31 μm with a projected baseline length of 10.4 m and a spectral resolution of 12 000.

Results. The uniform-disk diameter observed in the CO first overtone lines is 20−35% larger than is measured in the continuum. We have also detected a signature of inhomogeneities in the CO-line-forming region on a spatial scale of ∼45 mas, which is more than twice as large as the angular diameter of the star itself. While the MARCS photospheric model reproduces the observed spectrum well, the angular size in the CO lines predicted by the MARCS model is significantly smaller than observed. This is because the MARCS model with the parameters of Aldebaran has a geometrical extension of only ∼2% (with respect to the stellar radius). The observed spectrum and interferometric data in the CO lines can be simultaneously reproduced by placing an additional CO layer above the MARCS photosphere. This CO layer is extended to $2.5 \pm 0.3\ R_\star$ with CO column densities of 5×10^{19}−2×10^{20} cm^{-2} and a temperature of 1500 ± 200 K.

Conclusions. The high spectral resolution of AMBER has enabled us to spatially resolve the inhomogeneous, extended outer atmosphere (MOLsphere) in the individual CO lines for the first time in a K giant. Our modeling of the MOLsphere of Aldebaran suggests a rather small gradient in the temperature distribution above the photosphere up to 2−3 $R_\star$.

Key words. infrared: stars – techniques: interferometric – stars: mass-loss – stars: late-type – stars: atmospheres – stars: individual: Aldebaran

1. Introduction

Red giant stars, which represent the late evolutionary stages of intermediate- to low-mass stars from the red giant branch (RGB) to the asymptotic giant branch (AGB), experience mass loss ranging from 10^{-11} $M_\odot$ yr^{-1} up to 10^{-4} $M_\odot$ yr^{-1}. However, the mass loss in red giants is not yet understood well. For Mira-type AGB stars with large variability amplitudes ($\Delta V \approx 9$), the combination of the levitation of the atmosphere by the stellar pulsation and the radiation pressure on dust grains is often believed to drive the mass loss (see, e.g., Höfner 2011 for discussion of the success and the current problem with this mechanism). However, it is by no means clear whether this mechanism can operate in red giants in general, that is, normal (i.e., non-Mira-type) K and M giants, whose variability amplitudes ($\Delta V \approx 1$−2) are significantly smaller than Miras. Furthermore, K giants and early M giants are experiencing mass loss, despite the absence of dust.

Observations of the outer atmosphere are important for understanding the mass-loss mechanism. Infrared spectroscopic studies of molecular lines reveal the presence of an extended molecular outer atmosphere, the so-called MOLsphere, in K and M giants, as well as in red supergiants (Tsuji 1988, 2000a, 2000b, 2001; Tsuji et al. 1997). Spectro-interferometry, which combines high spectral resolution and high spatial resolution, is powerful for studying the physical properties of the MOLsphere.

We spatially resolved the normal M7 giant BK Vir in the CO first overtone lines near 2.3 μm with a spectral resolution of 12 000 using VLTI/AMBER (Ohnaka et al. 2012). The observed CO line spectrum can be reproduced well by the MARCS photospheric models (Gustafsson et al. 2008), which are state-of-the-art models for the photosphere of cool evolved stars. However, the MARCS models clearly fail to explain the observed angular size of the star in the individual CO lines. The observed angular size in the CO lines is much greater than the models predict, suggesting the presence of more extended components. We found out that the observed spectrum and angular size can be explained by a model in which two extra CO layers are added above the MARCS model photospheres, at 1.2−1.25 $R_\star$ and 2.5−3 $R_\star$ with CO column densities of 10^{22} cm^{-2} and 10^{19}−10^{20} cm^{-2}. Surprisingly, the temperatures of the CO layers (1900−2100 K and 1500−2100 K) are higher than or equal to the temperature of the uppermost layer of the photosphere (see Fig. 9 of Ohnaka et al. 2012). While many K and M giants possess chromospheres, the derived temperatures of the MOLsphere are still lower than in the chromosphere (∼6000−10 000 K). Therefore, although the MOLsphere shows a temperature inversion, it is still different from the chromosphere.

A better understanding of the physical properties of the MOLsphere is important for clarifying the mass-loss mechanism, because the physical process responsible for

⋆ Based on AMBER observations made with the Very Large Telescope Interferometer of the European Southern Observatory. Program ID: 090.D-0459(A).

Table 1. Summary of the AMBER observation of Aldebaran with the B2-C1-D0 AT configuration.

Night	t_{obs} (UTC)	B_p (m)	PA (°)	Seeing (″)	τ_0 (ms)	Airmass	DIT (ms)	Number of frames
Aldebaran								
2012 Dec. 12	05:18:32	31.1/10.4/20.7	37/37/37	0.64	4.4	1.45	121	500
Procyon (calibrator)								
2012 Dec. 12	05:40:16	28.1/9.4/18.7	22/22/22	0.98	2.9	1.21	121	2500

Notes. The seeing and coherence time (τ_0) are in the visible.

forming the MOLsphere may be related to the driving mechanism of the mass loss. Given that IR spectro-interferometric observations of normal K and M giants are still scarce, AMBER observations of more normal red giants are indispensable for shedding new light on the origin of the MOLsphere.

As a first step, we present a high-spatial and high-spectral resolution observation of the CO first overtone lines in the well-studied K5 giant Aldebaran (α Tau) with VLTI/AMBER. At a distance of 20.4 pc (parallax = 48.94 mas, van Leeuwen 2007), Aldebaran is one of the nearby red giants. Its angular diameter has been measured by the lunar occultation and long-baseline optical/IR interferometry. As summarized in Richichi & Roccatagliata (2005), most of the angular diameter measurements between the V and L band indicate 18−22 mas but without a noticeable wavelength dependence. As discussed in their paper, the scatter in the measured angular diameters mostly reflects the discrepancies among the lunar occultation measurements, and the scatter among the diameters measured by long-baseline interferometry is smaller. In the present work, we adopt the uniform-disk diameter of 19.96 ± 0.03 mas derived by Richichi & Roccatagliata (2005), which is the average of their lunar occultation measurements at 2.22 and 3.55 μm and the VLTI/VINCI measurements in the K band. They argue that their measurements would represent the best available value for the angular diameter of Aldebaran. We adopt an effective temperature ($T_{\rm eff}$) of 3874 ± 100 K and a stellar mass ($M_\star$) = 1.5 ± 0.3 $M_\odot$ from Tsuji (2008) for the present work. Combining this stellar mass and the radius of 44 $R_\odot$ measured by Richichi & Roccatagliata (2005) results in a surface gravity of $\log g$ = 1.5 (in units of cm s^{-2}). The metallicity of Aldebaran is solar or marginally subsolar with [Fe/H] = −0.14 ± 0.30 (Kovács 1983) and −0.15 ± 0.2 (Decin et al. 2003). Based on high-resolution spectra in the H, K, and L bands, Tsuji (2008) derived the carbon, nitrogen, and oxygen abundances to be $\log A_C = 8.38 \pm 0.04$, $\log A_N = 8.05$, and $\log A_O = 8.79 \pm 0.04$ (abundances are expressed on the logarithmic scale with $\log A_H = 12$). These CNO abundances suggest the mixing of the CN-cycled material in the first dredge-up, although the derived $^{12}C/^{13}C$ ratio of 10 cannot be fully understood by the standard evolutionary theory. The micro-turbulent velocity derived in previous studies is approximately 2 km s^{-1} (Smith & Lambert 1985; Decin et al. 2003; Tsuji 2008). The mass-loss rate and the terminal wind velocity of Aldebaran are estimated to be $(1-1.6) \times 10^{-11}$ $M_\odot$ yr^{-1} (Robinson et al. 1998; Wood et al. 2007) and 30 km s^{-1} (Robinson et al. 1998), respectively.

Tsuji (2001) discovered the H_2O absorption feature at ∼6.6 μm in Aldebaran, which originates in the MOLsphere. Based on a detailed analysis of a high-resolution spectrum of Aldebaran, Tsuji (2008) revealed absorption excess in the strong CO first overtone lines, which is also interpreted as the contribution of the MOLsphere. On the other hand, the emission lines in the UV (e.g., Mg II, Fe II, and O I lines) indicate the presence of the chromosphere. This inhomogeneous, multi-component nature of the outer atmosphere is consistent with what is suggested from the observations of the CO fundamental lines in the IR (Wiedemann et al. 1994) and the CO fluorescent lines in the UV (McMurry & Jordan 2000). Note, however, that the nature of the CO gas probed by the 4.6 μm fundamental lines (v = 1−0) might be different from that probed by the first overtone lines (v = 2−0) near 2.3 μm in the present work. The spectral energy distribution (SED) of Aldebaran from the optical to ∼1 mm, as well as the mid-IR spectrum shows no signature of dust (Dehaes et al. 2011; Monnier et al. 1998), and therefore, this star is ideal for studying the mass-loss mechanism without dust.

2. Observation

AMBER is a spectro-interferometric instrument at VLTI and can provide high spatial resolutions and high spectral resolutions of up to 12 000 (Petrov et al. 2007) by combining three 8.2 m Unit Telescopes (UTs) or 1.8 m Auxiliary Telescopes (ATs). AMBER measures the visibility, which is the amplitude of the Fourier transform of the object's intensity distribution on the sky, as well as the closure phase and differential phase. The closure phase contains information about the asymmetry of the object, with non-zero and non-π closure phases being the signature of asymmetry. The differential phase provides information about the photocenter shift of the object in spectral features with respect to the continuum.

We observed Aldebaran on 2012 December 12 with AMBER using the B2-C1-D0 (11−23−34 m) linear array (Program ID: 090.D-0459A, P.I.: K. Ohnaka), as summarized in Table 1. We used the high-spectral resolution mode in the K band (HR_K) with a spectral resolution of 12 000 between 2.28 and 2.31 μm to observe the CO first overtone lines near the 2−0 band head at 2.294 μm. The VLTI fringe tracker FINITO was not used, because while the visibility in the H band, where FINITO operates, is higher than the limit of 0.15 on the shortest baseline, the H-band visibility on the second shortest baseline is below the limit. However, the high brightness of Aldebaran enabled us to detect fringes without FINITO with a detector integration time (DIT) of 121 ms. We observed Procyon (F5IV-V) not only as the interferometric calibrator but also as the spectroscopic calibrator.

We reduced the data using amdlib ver.3.0.5[1] as described in Ohnaka et al. (2009). We took the best 80% of the frames in terms of the fringe S/N (Tatulli et al. 2007). For the calibrator Procyon, we adopted the uniform-disk diameter of 5.38 ± 0.05 mas from the CHARM2 catalog (Richichi et al. 2005). There are two issues that had to be taken into account in the reduction of the present data. Firstly, the telescope at the D0 station was shadowed by UT1 during the observation of Aldebaran (but not during the observation of Procyon). Therefore, the flux

[1] Available at http://www.jmmc.fr/data_processing_amber.htm

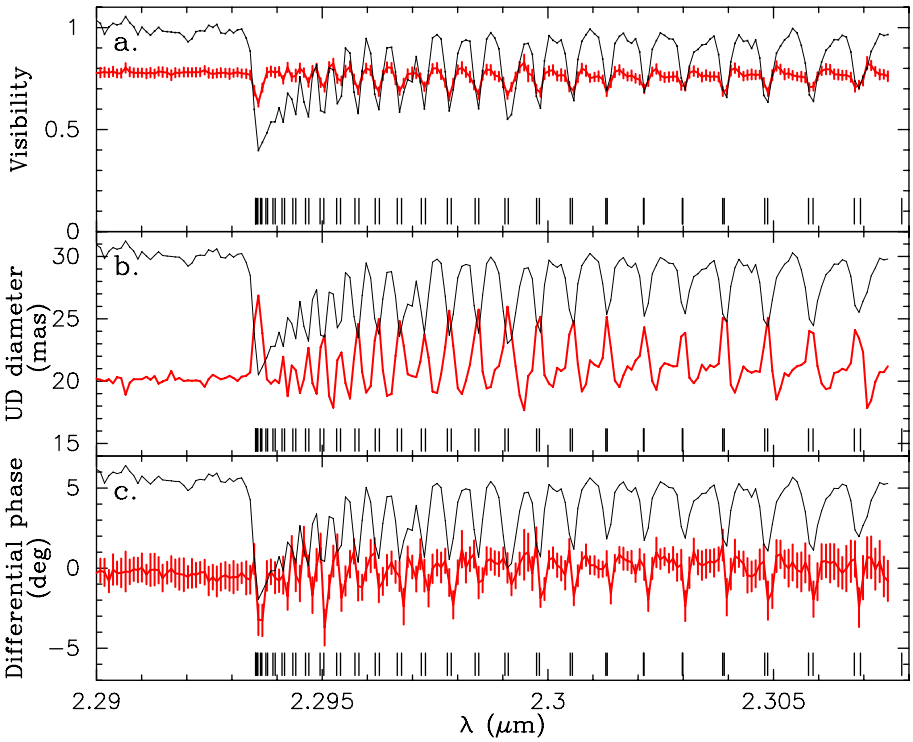

Fig. 1. AMBER observation of Aldebaran in the CO first overtone lines. **a)** Visibility observed on the 10.4 m baseline (red solid line). **b)** Uniform-disk (UD) diameter (red solid line). **c)** Differential phase (red solid line). In each panel, the scaled observed spectrum is shown by the black solid line. The positions of the CO lines are also marked with the ticks.

of Aldebaran at this telescope was lower than at the other two telescopes by a factor of ∼10, which makes the derivation of the interferometric observables on the baselines including the D0 telescope less reliable. Therefore, in the present work, we only discuss the visibility and differential phase obtained on the B2−C1 baseline, which provides a projected baseline length (B_p) of 10.4 m and a position angle (PA) of 37°. Secondly, only one data set of the calibrator was obtained, which makes it difficult to carry out a reliable calibration of the absolute visibility level. Because the time variation expected in the angular diameter of Aldebaran is as small as ±0.17 mas (Richichi & Roccatagliata 2005), we scaled the observed calibrated visibility in the continuum to those expected from a uniform disk with the adopted angular diameter of 19.96 mas.

The wavelength calibration was carried out using the telluric lines identified in the observed spectrum of Procyon, as described in Ohnaka et al. (2012). The uncertainty in the wavelength calibration is 3.2×10^{-5} μm (4.2 km s^{-1}). The wavelength scale was converted to the laboratory frame using a heliocentric velocity of 54.2 km s^{-1} of Aldebaran (Gontcharov 2006). The spectrum of Procyon in the observed spectral window is featureless with AMBER's spectral resolution except for the Mg line at 2.2814 μm. Therefore, the calibrated spectrum of Aldebaran was obtained by dividing the observed spectrum of Aldebaran with that of Procyon.

3. Results

Figure 1a shows the observed visibility in the CO lines on the 10.4 m baseline with the observed (spatially unresolved) spectrum. The signature of the CO lines is clear in the observed visibility. The uniform-disk diameter derived from the visibility is shown in Fig. 1b. The uniform-disk diameter in the CO lines is 20−35% larger than in the continuum. Figure 1c shows the observed differential phase. We detect non-zero differential phases in the CO lines (i.e., wavelength-dependent photocenter shifts), which indicate the presence of asymmetric or inhomogeneous structures in the CO-line-forming region on a spatial scale of ∼45 mas (corresponding to the spatial resolution with the 10.4 m baseline). This is more than twice as large as the angular diameter of the star itself and consistent with the size of the MOLsphere as discussed in Sect. 4. Richichi & Roccatagliata (2005) found possible surface structures−though not conclusive as the authors mention−in the 1D image of Aldebaran reconstructed from the lunar occultation data taken at 2.22 μm with a spectral resolution of ∼70, which sample the spectral region free from strong lines. Our AMBER observation is the first study to spatially resolve the atmosphere of a K giant in individual CO lines and detect asymmetry in the CO-line-forming region.

The observed increase in the uniform-disk diameter in the CO lines is in marked contrast to the negative detection of a change in the angular size in the TiO band at 7120 Å (Quirrenbach et al. 1993). However, this might be due to the lower spectral resolution used in their observations. For example, if we bin our AMBER data to a spectral resolution of 1500 as described in Ohnaka et al. (2009), the increase in the uniform-disk diameter in the CO band head is 4%. The narrow-band filter for the TiO band used by Quirrenbach et al. (1993) has a spectral resolution of ∼60. The width of the filter (120 Å) is smaller than the width of the TiO band (∼400 Å) starting at ∼7050 Å. However, the observed spectrum of Aldebaran in Kieling (1987, Fig. 4c, HR 1457 = Aldebaran) shows that this TiO band is centered at 7200 Å, and the central wavelength of the filter (7120 Å) does not exactly match the center of the TiO band. The filter samples the spectral region between the beginning and the center of the TiO band, not just the deepest part of the TiO band. Therefore, the low spectral resolution, as well as the shift between the filter's central wavelength and the center of the TiO band, might have led to the negative detection of the extended atmosphere of Aldebaran. It might not have been a problem for detecting a change in the angular size for cooler stars with more pronounced extended atmospheres. In any case, measurements of the angular diameter of K giants in

the TiO bands with higher spectral resolutions are necessary to compare with the angular diameter in the CO first overtone lines. This can be feasible, for example, with the visible interferometric instrument VEGA at CHARA with spectral resolutions of up to 30 000 (Mourard et al. 2009).

The high spatial and high spectral resolution of AMBER has enabled Ohnaka et al. (2009, 2011, and 2013) to spatially resolve the gas motions in the photosphere and MOLsphere in the red supergiants Betelgeuse and Antares. However it is difficult to carry out a similar analysis for the current data of Aldebaran, because the amplitude of the velocity field in the photosphere (and possibly also in the MOLsphere) is much smaller than in the red supergiants. For example, Gray (2009) measured a time variation in the radial velocity of ± 0.3 km s^{-1} in Aldebaran, which is much smaller than the amplitude of $\sim$7 km s^{-1} found in Betelgeuse (Gray 2008). The micro- and macro-turbulent velocities of $\sim$2 km s^{-1} and 3.6 ± 0.3 km s^{-1} derived for Aldebaran (references given in Sect. 1 and Tsuji 1986) are also noticeably smaller than the micro- and macro-turbulent velocities of $\sim$5 and 10–20 km s^{-1} in Betelgeuse (Ohnaka et al. 2009 and references therein). The amplitude of the velocity field suggested from these observations is too small compared to AMBER's spectral resolution and the accuracy of the wavelength calibration.

4. Modeling the AMBER data

We first compare the observed spectrum and visibility with the MARCS photospheric model (Gustafsson et al. 2008). The MARCS models represent plane-parallel or spherical photospheres in hydrostatic and radiative equilibrium, with the effects of molecular and atomic line opacities included using the opacity sampling method. Each MARCS model is specified by effective temperature ($T_{\rm eff}$), surface gravity ($\log g$), micro-turbulent velocity ($v_{\rm micro}$), chemical composition, and (for the spherical case) stellar mass ($M_\star$). We selected spherical MARCS models with $T_{\rm eff}$ = 3900 K, $\log g$ = 1.5, $M_\star$ = 1 and 2 $M_\odot$ (no MARCS model with 1.5 $M_\star$ is available), $v_{\rm micro}$ = 2 km s^{-1}, and the "moderately CN-cycled" composition with [Fe/H] = 0.0, because these models have the parameters closest to those of Aldebaran summarized in Sect. 1.

Using the temperature and pressure distributions from the MARCS models, we computed the monochromatic intensity profile and visibility, as well as the spectrum using the CO line list of Goorvitch (1994), as described in Appendix A. The angular scale of the models was determined so that the uniform-disk diameter derived from the model visibility in the continuum agrees with the adopted value of 19.96 mas.

Comparison of the MARCS model visibility and spectrum with the AMBER observation is shown in Fig. 2. The observed CO line spectrum (Fig. 2a) is reproduced well by the MARCS model with $T_{\rm eff}$ = 3900 K, $\log g$ = 1.5, and $M_\star$ = 1 $M_\odot$. However, as Figs. 2b and 2c show, the model predicts only marginal decrease in the visibility (thus only marginal increase in the uniform-disk diameter) in the CO lines and fails to explain the observed data. This means that the star is much more extended than the MARCS model predicts. The geometrical extension of the MARCS model, which is defined as the geometrical distance between the layers with $\tau_{\rm Ross}$ = 1 and $\tau_{\rm Ross}$ = 10^{-5} ($\tau_{\rm Ross}$ is the optical depth based on the Rosseland mean opacity), is 2% of the stellar radius. This geometrically thin photosphere is seen in Fig. 2d, where the intensity profiles in the continuum and in the CO band head are shown. This means that the visibilities predicted in the continuum and in the CO band head differ only slightly (Fig. 2e). This is why the MARCS model cannot explain the increase in the uniform-disk diameter of 20–35% in the CO lines. We also examined whether MARCS models with slightly different parameters can explain the observed visibility. However, the MARCS models with $T_{\rm eff}$ = 3800–4000 K, $\log g$ = 1.0 and 1.5, and $M_\star$ = 1 and 2 $M_\odot$ are characterized by the geometrical extension of 4% at most, and therefore, cannot explain the observed significant increase in the angular size in the CO lines. This finding that the MARCS model can reproduce the CO first overtone line spectrum well but fails to explain the angular size of the star in the CO lines is the same as what we found in the M7 giant BK Vir in Ohnaka et al. (2012). Our AMBER observation with high spectral resolution has clearly

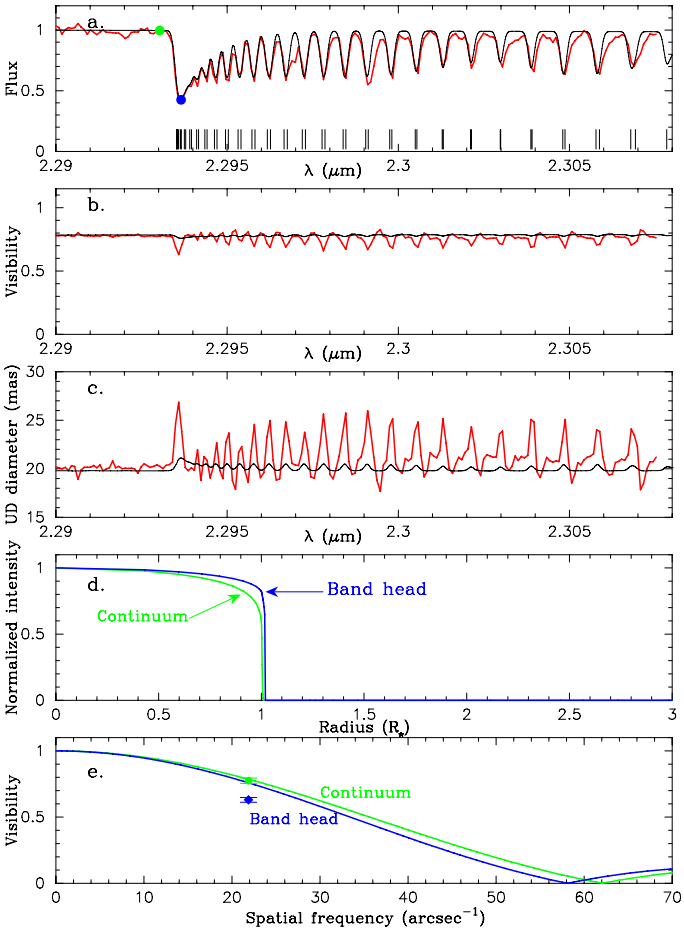

Fig. 2. Comparison of the MARCS model with the AMBER data of Aldebaran. The parameters of the MARCS model are given in Sect. 4. **a)** Model spectrum (black solid line) computed from the pressure and temperature distributions of the MARCS model as described in Appendix A (not the pre-computed spectrum available on the MARCS website) with the observed spectrum (red solid line). The green and blue dots show the wavelengths of the intensity profiles and visibilities shown in the panels **d)** and **e)**. The positions of the CO lines are marked by the ticks. **b)** Model visibility predicted at the 10.4 m baseline (black solid line) with the observed data (red solid line). **c)** Uniform-disk (UD) diameter derived from the MARCS model visibility shown in the panel **b)** (black solid line) with the one observed (red solid line). **d)** Model intensity profiles predicted in the continuum (green solid line) and in the CO band head (blue solid line), at the wavelengths marked in the panel **a)**. **e)** Model visibilities as a function of spatial frequency predicted in the continuum (green solid line) and in the CO band head (blue solid line). The visibilities observed at these wavelengths are plotted by the dot (continuum) and the filled diamond (CO band head).

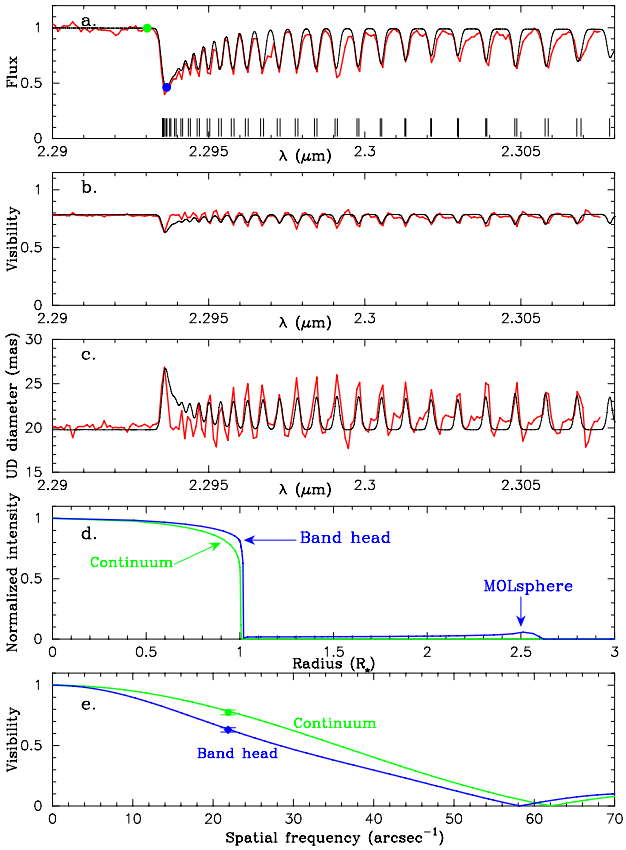

Fig. 3. Comparison of the MARCS+MOLsphere model with the AMBER data of Aldebaran shown in the same manner as in Fig. 2.

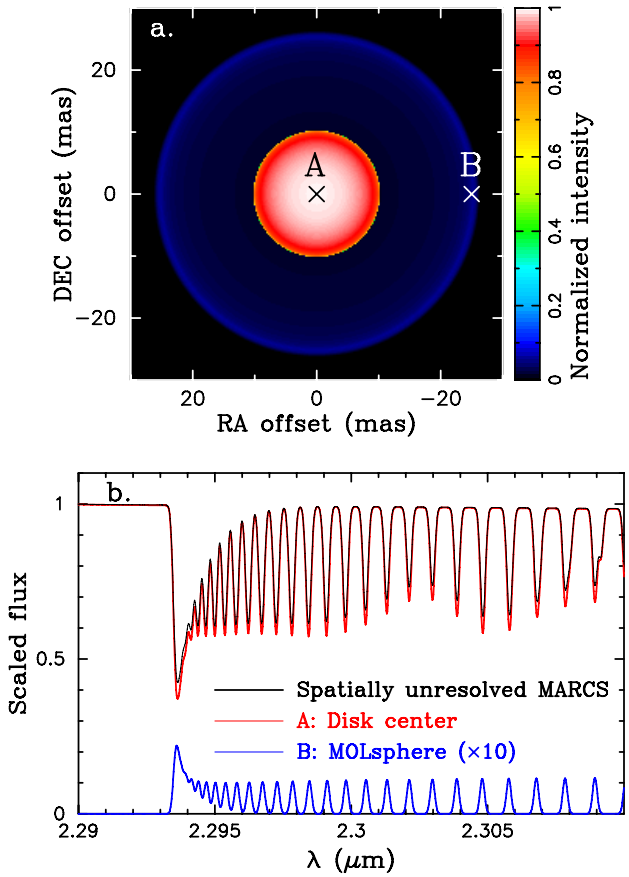

Fig. 4. **a)** The image predicted at the CO band head by the MARCS+MOLsphere model shown in Fig. 3. **b)** Spatially resolved spectra at the center of the stellar disk (position A in the panel **a**) and at the edge of the MOLsphere (position B) are shown by the red and blue solid line, respectively. The spatially unresolved spectrum from the MARCS-only model is plotted by the black solid line. The spectrum at the edge of the MOLsphere is scaled up by a factor of 10.

revealed the presence of the MOLsphere, which cannot be accounted for by the photospheric models.

We derived the physical properties of the MOLsphere using the model described in Ohnaka et al. (2012). In this model, one or two CO layers are added above the MARCS photospheric model. Given that the visibility was obtained only on one baseline in the present work, we used only one layer to keep the number of free parameters as small as possible. The geometrical thickness of the additional CO layer is fixed to 0.1 $R_\star$, and the micro-turbulent velocity in the CO layer is set to 2 km s^{-1}, which is the same as in the MARCS photospheric model. The (inner) radius, CO column density in the radial direction, and temperature of the CO layer were treated as free parameters. The computation of the intensity profile, visibility, and spectrum from the MARCS+MOLsphere model is described in Appendix A.

Figure 3 shows a comparison of the best-fit MARCS+MOLsphere model with the observed spectrum and visibility. The MOLsphere of this model is characterized by a radius of 2.5 $R_\star$ with a temperature of 1500 K and a CO column density of 1×10^{20} cm^{-2}. The observed spectrum and visibility, as well as the uniform-disk diameter are reasonably reproduced. The intensity profile shown in Fig. 3d reveals the extended emission from the MOLsphere. While the intensity of this extended emission is low compared to the intensity on the stellar disk, the flux contribution is not negligible because it is very extended. As a result, the MOLsphere makes the star appear much more extended than the photosphere alone and can explain the observed angular size in the CO lines. We computed MOLsphere models with radii between 1.2 and 2.8 $R_\star$, temperatures between 1000 and 2000 K, and CO column densities between 1×10^{19} and 1×10^{21} cm^{-2}, and estimate the uncertainties in the radius, temperature, and CO column density to be ±0.3 $R_\star$, ±200 K, and a factor of 2, respectively.

It may appear contradictory that the model spectrum is hardly affected by the MOLsphere, while the angular size is largely affected. This can be explained as follows. Figure 4 shows spatially resolved spectra predicted at two positions (at the center of the stellar disk and at the edge of the MOLsphere) by the MARCS+MOLsphere model, together with the spatially unresolved model spectrum. On the one hand, the additional CO layer introduces stronger absorption (i.e., CO absorption lines are deeper) for lines of sight within the stellar disk. This can be seen in the spatially resolved spectrum at the stellar disk center (red line) when compared to the spatially unresolved spectrum from the MARCS-only model (black line). On the other hand, the spatially resolved spectrum at the edge of the MOLsphere (blue line) shows that the CO lines appear in emission off the limb of the star (note that the off-limb spectrum is scaled up by a factor of 10 for visual clarity). This extended emission from the MOLsphere fills in the additional absorption due to the MOLsphere itself, which results in little change in the spatially unresolved spectrum. The spectra predicted by the MARCS-only and MARCS+MOLsphere models shown in Figs. 2a and 3a show very little difference. However, the difference in the visibility predicted by these models is obvious. This illustrates that the MOLsphere can become invisible for a

spectrometer but not for a spectro-interferometer (however, signatures of the MOLsphere can be detected by spectroscopy for some lines, as demonstrated by Tsuji 2001, 2008). It is also feasible to observe the CO emission line spectrum expected from the MOLsphere, if we carry out aperture-synthesis imaging with high-spectral resolution with AMBER, as demonstrated for the red supergiants Betelgeuse and Antares (Ohnaka 2013; Ohnaka et al. 2013).

We assumed local thermodynamical equilibrium (LTE) for modeling the MOLsphere. We examined whether this assumption is valid for the derived density and temperature of the MOLsphere. As described in Ohnaka (2004), we compared the collisional and radiative de-excitation rates. The collisional de-excitation rate $C_{\rm ul}$ is estimated as $N\sigma_{\rm ul}\upsilon_{\rm rel}$, where N, $\sigma_{\rm ul}$, and $\upsilon_{\rm rel}$ denote the number density of the primary collision partner, collisional cross section, and relative velocity between the collision partner and CO molecules. We approximate $\sigma_{\rm ul}$ with the geometrical cross section of 10^{-15} cm^2 and adopt $\upsilon_{\rm rel}$ = 5 km s^{-1}. The number density of the primary collision parter (H_2 or H) is estimated as follows. We estimate the CO number density by dividing the derived CO column density by the geometrical thickness of the MOLsphere. However, we arbitrarily set the geometrical thickness to 0.1 $R_\star$ because this parameter cannot be constrained from the current data. Therefore, we estimated a lower limit on the CO number density by dividing the derived CO column density (10^{20} cm^{-2}) by the geometrical distance between the stellar surface and the radius of the MOLsphere. This results in a CO number density of 2.2×10^7 cm^{-3}. In chemical equilibrium at 1500 K, this CO number density suggests H_2 and H number densities of 5.6×10^{10} and 9.5×10^9 cm^{-3}, respectively. Using the H_2 number density for N, we obtain $C_{\rm ul} = 2.8 \times 10$ s^{-1}. This collisional de-excitation rate is much higher than the radiative de-excitation rates $A_{\rm ul}$ = 0.6−1 s^{-1}. Therefore, it is unlikely that our modeling is significantly affected by NLTE effects.

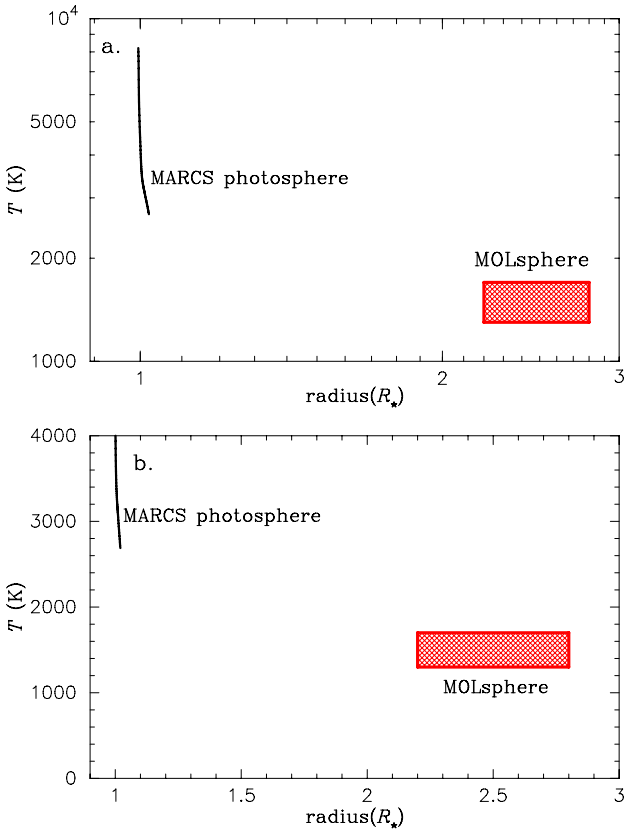

Fig. 5. Temperature distribution as a function of radius predicted by the MARCS model for Aldebaran (black solid line) and the temperature of the MOLsphere derived from our modeling (red hatched rectangle). The panel **a)** shows the entire temperature range covered by the MARCS photosphere (note the logarithmic scale both for the temperature and radius), while the panel **b)** shows a lower temperature region including the upper photosphere and MOLsphere on the linear scale.

5. Discussion

Our modeling of the spatially and spectrally resolved CO line data suggests a high CO column density in the MOLsphere of Aldebaran. Tsuji (2001) estimated an H_2O column density of 2×10^{17} cm^{-2} from the weak absorption feature near 6.6 μm. The CO number density estimated above suggests an H_2O column density of 1.4×10^{20} cm^{-2}, if we assume chemical equilibrium at 1500 K. The H_2O column density implied from our modeling of the CO lines is much higher than estimated from the previous spectroscopic study. A possible reason for this disagreement may be that it is not straightforward to disentangle the effects of the geometrical extension and column density from the observed spectra alone.

Based on the spectral analysis of the CO fluorescent lines in the UV, McMurry & Jordan (2000) deduced the inhomogeneous structure of the atmosphere of Aldebaran: the chromosphere as hot as 10^4 K extending into the transition region with 10^5 K and the cool CO gas at ∼2000 K. This temperature of the cool CO gas is comparable to the temperature of the MOLsphere derived above. However, the CO column density derived by McMurry & Jordan (2000) is $\sim 1 \times 10^{17}$ cm^{-2}, which is much lower than derived for the MOLsphere. We computed MARCS+MOLsphere models with the CO column density fixed to 1×10^{17} cm^{-2}, but the angular size in the CO lines predicted by these models is too small compared to the observed data, simply because the density is too low. Therefore, this discrepancy in the CO column density cannot be reconciled by adjusting the parameters in our modeling of the MOLsphere. Instead it may be related to the location where the CO fluorescent lines originate. The CO fluorescent lines in the UV are pumped by the O I lines that form in the chromosphere at temperatures of 6500−8000 K (McMurry 1999; McMurry & Jordan 2000). The spectral analysis of the latter authors implies that "the O I radiation and CO molecules must be in close proximity". Therefore, the CO column density derived from the fluorescent lines may refer only to the cool CO gas near the hot chromospheric gas, while the CO column density estimated from the CO first overtone lines refers to the entire cool CO gas.

Figure 5 shows the temperature distribution of the MARCS model for Aldebaran and the temperature and location of the MOLsphere derived from our modeling. Compared to the steep temperature decrease in the photosphere, the temperature gradient in the outer atmosphere is much smaller. This is similar to what was found in the M7 giant BK Vir, in which the temperature in the MOLsphere is equal to or even higher than in the uppermost layer of the MARCS model (Ohnaka et al. 2012). The CO column density in the MOLsphere of Aldebaran is comparable to the value found in the red supergiants Betelgeuse (Ohnaka et al. 2009, 2011) and Antares (Ohnaka et al. 2013), as well as BK Vir (Ohnaka et al. 2012), despite the higher effective temperature and higher surface gravity of Aldebaran. This implies that the physical process responsible for the formation of the MOLsphere may be the same for red supergiants and (non-Mira) red giants regardless the spectral type and luminosity class.

To shed new light on the origin of the MOLsphere, the magnetohydrodynamical (MHD) simulation of Suzuki (2007) is interesting for the present study. In particular, his model IV has stellar parameters similar to Aldebaran: $T_{\rm eff}$ = 3900 K, $M_\star$ = 1 $M_\odot$, $R_\star$ = 31 $R_\odot$, and log g = 1.4. He simulates Alfvén waves, which are excited by the surface convection and travel outward along an open 1D magnetic flux tube from the photosphere to ∼25 $R_\star$. The simulation also solves the thermal structure of the wind, instead of assuming a given temperature profile. The magnetic field used in the simulation corresponds to a surface-averaged magnetic field strength of 1 G. The stellar wind of the model IV shows hot gas bubbles with a temperature higher than $\sim 10^5$ K embedded in much cooler gas. A snapshot of the temperature structure (see Fig. 9 in his paper) shows that the temperature in the cool gas can be as low as 1000−2000 K, which agrees with the observationally derived temperature of the MOLsphere. The model also show hot gas bubbles with temperatures of 10^4−10^5 K, which may correspond to the chromosphere or the "buried" corona as Ayres et al. (2003) propose. The lower limit on the CO number density of 2.2×10^7 cm^{-3} derived above suggests a gas density of 1.9×10^{-13} g cm^{-3}. The time-averaged gas density predicted at 2 $R_\star$ for the model IV is $\sim 10^{-14}$ g cm^{-3}. Given the large temporal fluctuation in the density structure predicted by the model (by a factor of 10−100) and the uncertainty in the observationally derived CO column density, this value roughly agrees with the observationally estimated density.

However, the time-averaged mass-loss rate predicted by this model is $\sim 10^{-9}$ $M_\odot$ yr^{-1}, which is significantly higher than the observationally estimated value of (1−1.6) × 10^{-11} $M_\odot$ yr^{-1} (Robinson et al. 1998; Wood et al. 2007), although the model is not constructed particularly for Aldebaran. Also, as pointed out by Airapetian et al. (2010), the fully ionized plasma is assumed, while the winds from red giants are weakly ionized. While the MHD simulation of the stellar wind of Aldebaran by Airapetian et al. (2010) assumes weakly ionized plasma, the temperature structure is not self-consistently computed in their simulation, and therefore, their model cannot yet account for the MOLsphere component. Another uncertainty in the MHD models is that the strength of the magnetic fields in Aldebaran is not observationally determined. On the one hand, the detection of O VI emission lines suggests that the outer atmosphere of Aldebaran is influenced by magnetic fields (Harper et al. 2011). On the other hand, the spectropolarimetric observations of Aurière et al. (2010) detected no signature of magnetic fields in Aldebaran, implying that the surface-averaged field strength is much smaller than the 1 G in the model. An extension of the MHD simulations of Suzuki (2007) with weaker magnetic fields and weakly ionized plasma, as well as the inclusion of the MOLsphere component in the model of Airapetian et al. (2010) would be crucial for comparison with the observed data.

McMurry & Jordan (2000) propose an alternative scenario, in which the hot chromospheric gas is associated to acoustic shocks. The one-dimensional simulation of acoustic waves for a K5 giant (corresponding to Aldebaran) by Buchholz et al. (1998) shows that while the temperature behind shocks can become higher than ∼5000 K, the gas between shocks can be as cool as 2000 K. However, the cooling due to molecules (most importantly CO) is not included in their simulation. A more realistic simulation of acoustic waves including the molecular cooling is necessary to understand the formation mechanism of the chromosphere and MOLsphere.

While our MARCS+MOLsphere model simultaneously explains the spectrum and angular size in the CO lines of Aldebaran, there is still a problem with the MOLsphere as mentioned by Ohnaka et al. (2012) for the M7 giant BK Vir. A large number of other molecular species is expected from the MOLsphere, most notably TiO. The contribution of TiO in the MOLsphere can make the TiO absorption bands too strong compared to the observed spectra. Ohnaka et al. (2012) suggest that the TiO bands may form by scattering in the MOLsphere, and the scattered emission may fill in the absorption caused by the MOLsphere. However, it is necessary to construct a MOLsphere model with the scattering taken into account and compare it with the observed spectra and the available and future angular diameter measurements in the TiO bands.

6. Conclusions

We have spatially resolved the K5 giant Aldebaran in the individual CO first overtone lines near 2.3 μm, taking advantage of high spatial and high spectral resolution of VLTI/AMBER. The observed uniform-disk diameter in the CO lines is 20−35% larger than in the continuum. This increase in the angular size in the CO features would be difficult to detect with a spectral resolution lower than ∼1500 (AMBER's medium spectral resolution mode). Our observation of Aldebaran illustrates the power of the high-spectral resolution capability of AMBER. While the MARCS photospheric model can reproduce the observed CO line spectrum very well, it fails to explain the observed angular diameter in the CO lines: the model predicts the angular diameter to be too small compared to the observation. This reveals the presence of the MOLsphere in a K giant for the first time in the individual CO lines. Our modeling of the AMBER data suggests that the MOLsphere extends to ∼2.5 $R_\star$ with a temperature of ∼1500 K and a CO column density of $\sim 1 \times 10^{20}$ cm^{-2}. The temperature gradient in the MOLsphere is much smaller than in the photosphere. The derived temperature and density of the MOLsphere roughly agree with the MHD simulation of Suzuki (2007), although a modeling with more appropriate assumptions for Aldebaran is necessary for understanding the origin of the MOLsphere.

Our work demonstrates that the high spatial and high spectral resolution of VLTI/AMBER enables us to extract unique information on the outer atmosphere even from data on only one baseline. Now it is crucial to carry out a systematic survey of red (super)giants with a range of effective temperature and luminosity with this technique for obtaining a more comprehensive picture of the dependence (or absence of it) of the properties of the MOLsphere on stellar parameters. This is possible with the current AMBER's sensitivity.

Acknowledgements. The author thanks the ESO VLTI team for supporting our AMBER observation and Karl-Heinz Hofmann for the fruitful discussion about the reduction of the AMBER data. The author also thanks the anonymous referee for his/her constructive comments.

Appendix A: Computation of the intensity profile, spectrum, and visibility from the MARCS+MOLsphere model

We first compute the monochromatic intensity profile only from a given MARCS model with a wavelength interval of 2.7 × 10^{-6} μm. This wavelength interval was chosen to sample at least 4−5 points across the line profile whose width is determined by the thermal and micro-turbulent velocity. As depicted

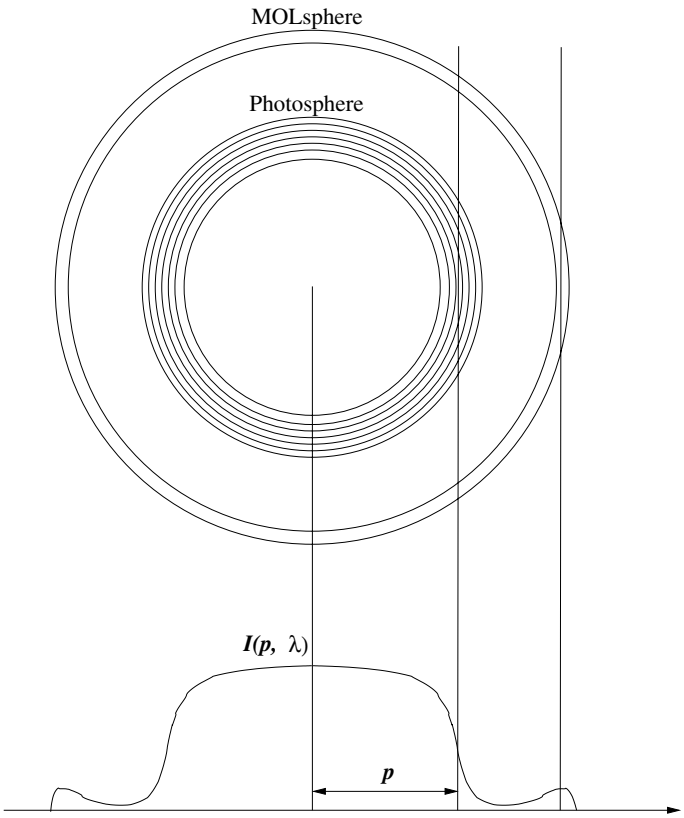

Fig. A.1. Schematic view of the computation of the intensity profile from the MARCS+MOLsphere model. Each MARCS model consists of 56 layers, but only six layers are drawn for the sake of clarity.

in Fig. A.1, the monochromatic intensity $I_{\rm MARCS}(p, \lambda)$ at the wavelength λ and at a given impact parameter (p) is obtained by

$$I_{\rm MARCS}(p, \lambda) = \int S_\lambda(\tau_\lambda)\, {\rm e}^{-\tau_\lambda}\, {\rm d}\tau_\lambda,$$

where S_λ and τ_λ denote the source function and the optical depth at λ along the ray with the impact parameter p, and the integration is carried out along this ray. In local thermodynamical equilibrium (LTE), the source function is given by

$$S_\lambda = \frac{\kappa_\lambda}{\kappa_\lambda + \sigma_\lambda} B_\lambda + \frac{\sigma_\lambda}{\kappa_\lambda + \sigma_\lambda} J_\lambda,$$

where κ_λ and σ_λ represent the absorption and scattering coefficients, respectively. B_λ and J_λ represent the Planck function and the mean intensity, respectively. From the pressure and temperature distributions of a given MARCS model, we compute the number of each molecular and atomic species in chemical equilibrium. With the Voigt function adopted for the line profile, the absorption coefficient at each wavelength is calculated from the CO line list of Goorvitch (1994) and the continuous opacities due to the bound-free and free-free transitions of H^- and H, the free-free transitions of H_2^- and He^-, and the bound-free transitions of Si, Mg, and Ca. We used the data of John (1988) for the H^- opacity, while we adopted the cross sections given in Tsuji (1971 and references therein) for the other continuous opacities.

The intensity profile from a MARCS+MOLsphere model $I_{\rm MARCS+MOL}(p, \lambda)$ is computed using the MARCS-only intensity profile $I_{\rm MARCS}(p, \lambda)$ as follows:

$$I_{\rm MARCS+MOL}(p, \lambda) = I_{\rm MARCS}(p, \lambda)\, {\rm e}^{-\tau_\lambda^{\rm MOL}} + B_\lambda(T_{\rm MOL})(1 - {\rm e}^{-\tau_\lambda^{\rm MOL}}),$$

where $\tau_\lambda^{\rm MOL}$ denotes the optical depth in the MOLsphere along the ray with the impact parameter p, and $T_{\rm MOL}$ is the temperature of the MOLsphere.

Once the intensity profile at each wavelength is obtained, the spectrum from the MARCS+MOLsphere model (F_λ) is calculated by

$$F_\lambda = 2\pi \int_0^1 I_{\rm MARCS+MOL}(p, \lambda)\, \mu\, {\rm d}\mu,$$

where μ is defined as $\sqrt{1 - (p/R_{\rm MOL})^2}$ with $R_{\rm MOL}$ being the outer radius of the MOLsphere. The visibility is obtained by taking the Hankel transform (2D Fourier transform for axisymmetric objects) of the intensity profile.

Finally, the monochromatic intensity profile and visibility, as well as the spectrum are spectrally convolved with the AMBER's spectral resolution.

References

Airapetian, V. S., Carpenter, K. G., & Ofman, L. 2010, ApJ, 723, 1210
Aurière, M., Donati, J.-F., Konstantinova-Antova, R., et al. 2010, A&A, 516, L2
Ayres, T., Brown, A., & Harper, G. M. 2003, ApJ, 598, 610
Buchholz, B., Ulmschneider, P., & Cuntz, M. 1998, ApJ, 494, 700
Decin, L., Vandenbussche, B., Waelkens, C., et al. 2003, A&A, 400, 709
Dehaes, S., Bauwens, E., Decin, L., et al. 2011, A&A, 533, A107
Gontscharov, G. A. 2006, Astron. Lett., 32, 759
Goorvitch, D. 1994, ApJS, 95, 535
Gray, D. F. 2008, AJ, 135, 1450
Gray, D. F. 2009, ApJ, 697, 1032
Gustafsson, B., Edvardsson, B., Eriksson, K., et al. 2008, A&A, 486, 951
Harper, G. M., Brown, A., & Redfield, S. 2011, in The 16th Cambridge Workshop on Cool Stars, Stellar systems and the Sun, ASP Conf. Ser., 448, E-1145
Höfner, S. 2011, in Why Galaxies Care About AGB stars II: Shining examples and common inhabitants, eds. F. Kerschbaum, T. Lebzelter, & R. Wing, ASP Conf. Ser., 445, 193
John, T. L. 1988, A&A, 193, 189
Kiehling, R. 1987, A&AS, 69, 465
Kovács, N. 1983, A&A, 120, 21
McMurry, A. D. 1999, MNRAS, 302, 37
McMurry, A. D., & Jordan, C. 2000, MNRAS, 313, 423
Monnier, J. D., Geballe, T. R., & Danchi, W. C. 1998, ApJ, 502, 833
Mourard, D., Clausse, J. M., Marcotto, A., et al. 2009, A&A, 508, 1073
Ohnaka, K. 2004, A&A, 424, 1011
Ohnaka, K. 2013, Proc. Betelgeuse Workshop 2012, The physics of Red Supergiants: recent advances and open questions, EAS Pub. Ser., in press
Ohnaka, K., Hofmann, K.-H., Benisty, M., et al. 2009, A&A, 503, 183
Ohnaka, K., Weigelt, G., Millour, F., et al. 2011, A&A, 529, A163
Ohnaka, K., Hofmann, K.-H., Schertl, D., et al. 2012, A&A, 537, A53
Ohnaka, K., Hofmann, K.-H., Schertl, D., et al. 2013, A&A, accepted
Petrov, R. G., Malbet, F., Weigelt, G., et al. 2007, A&A, 464, 1
Quirrenbach, A., Mozurkewich, D., Armstrong, J. T., Buscher, D. F., & Hummel, C. A. 1993, ApJ, 406, 215
Richichi, A., & Roccatagliata, V. 2005, A&A, 433, 305
Richichi, A., Percheron, I., & Khristoforova M. 2005, A&A, 431, 773
Robinson, R. D., Carpenter, K. G., & Brown, A. 1998, ApJ, 503, 396
Smith, V. V., & Lambert, D. L. 1985, ApJ, 294, 326
Suzuki, T. K. 2007, ApJ, 659, 1592
Tatulli, E., Millour, F., Chelli, A., et al. 2007, A&A, 464, 29
Tsuji, T. 1971, PASJ, 23, 553
Tsuji, T. 1986, A&A, 156, 8
Tsuji, T. 1988, A&A, 197, 185
Tsuji, T. 2000a, ApJ, 538, 801
Tsuji, T. 2000b, ApJ, 540, L99
Tsuji, T. 2001, A&A, 376, L1
Tsuji, T. 2008, A&A, 489, 1271
Tsuji, T., Ohnaka K., Aoki, W., & Yamamura, I. 1997, A&A, 320, L1
van Leeuwen, F. 2007, A&A, 474, 653
Wiedemann, G., Ayres, T. R., Jennings, D. E., & Saar, S. H. 1994, ApJ, 423, 806
Wood, B., Harper, G. M., Müller, H.-R., Heerikhuisen, J., & Zank, G. P. 2007, ApJ, 655, 946